

THE OFFICIAL MAGAZINE OF THE OCEANOGRAPHY SOCIETY

Oceanography

CITATION

Sakamoto, C.M., K.S. Johnson, L.J. Coletti, T.L. Maurer, G. Massion, J.T. Pennington, J.N. Plant, H.W. Jannasch, and F.P. Chavez. 2017. Hourly in situ nitrate on a coastal mooring: A 15-year record and insights into new production. *Oceanography* 30(4):114–127, <https://doi.org/10.5670/oceanog.2017.428>.

DOI

<https://doi.org/10.5670/oceanog.2017.428>

COPYRIGHT

This article has been published in *Oceanography*, Volume 30, Number 4, a quarterly journal of The Oceanography Society. Copyright 2017 by The Oceanography Society. All rights reserved.

USAGE

Permission is granted to copy this article for use in teaching and research. Republication, systematic reproduction, or collective redistribution of any portion of this article by photocopy machine, reposting, or other means is permitted only with the approval of The Oceanography Society. Send all correspondence to: info@tos.org or The Oceanography Society, PO Box 1931, Rockville, MD 20849-1931, USA.

HOURLY IN SITU NITRATE ON A COASTAL MOORING

A 15-Year Record and Insights into New Production



By Carole M. Sakamoto, Kenneth S. Johnson, Luke J. Coletti,
Tanya L. Maurer, Gene Massion, J. Timothy Pennington,
Joshua N. Plant, Hans W. Jannasch, and Francisco P. Chavez



ABSTRACT. Chemical sensor development has been a focus for the Monterey Bay Aquarium Research Institute (MBARI) from its inception. Progress in chemical analyzers benefited from technological advances in many fields. MBARI's development of a low power, reagent-free, in situ ultraviolet spectrophotometer (ISUS) for measuring dissolved nitrate has been transformative. These ultraviolet optical nitrate sensors have been deployed on remotely operated vehicles, autonomous underwater vehicles, benthic flux chambers, profiling floats, and moorings. This paper focuses on a 15+ year time series of nitrate observations on MBARI's M1 mooring in Monterey Bay, California. The resulting data set captures seasonal and interannual variability from El Niño and La Niña, and water mass anomalies on the eastern boundary of the Pacific Ocean. The high temporal resolution (hourly) nitrate measurements additionally quantify diel cycles of nitrate uptake as a proxy for new production. The calculated f-ratio varies seasonally with relatively higher values during the lower productivity winter season. The physical supply and uptake of nitrate are dominated by upwelling in this coastal environment. An expanding number of ultraviolet optical nitrate sensor deployments on moorings and autonomous platforms such as profiling floats will provide ever-broadening coverage of the world ocean, resulting in enhanced spatial and temporal resolution of nitrate measurements and, ultimately, improved insight into the dynamics of nitrogen cycling and phytoplankton ecology throughout a changing global ocean.

INTRODUCTION

In his welcoming remarks at The Oceanography Society's inaugural meeting in 1989, David Packard, Chairman of the Board of Hewlett-Packard Company and founder of the Monterey Bay Aquarium Research Institute (MBARI), shared his vision that Monterey Bay would become one of the major world-class centers for ocean science by applying technological innovation to oceanography. He felt that breakthroughs in science can come from breakthroughs in technology (*pers. comm.*), and to facilitate such advances, he established a management structure that ensures scientists and engineers work together and have personal contact on a daily basis (Packard, 1989).

One area of technology in which David Packard thought MBARI could advance scientific research was in instrumentation for chemical analysis (Packard,

1989). MBARI focused both on developing chemical sensors that could characterize the temporal and spatial distribution of biologically relevant parameters in the ocean and on platforms to enable the collection of extended oceanographic time-series observations. Results have included moorings and drifters (Chavez et al., 1997; Jannasch et al., 2008), chemical mapping systems (Sakamoto et al., 1996), automated oxygen titrators (Friederich et al., 1991), and nutrient analyzers (Plant et al., 2009), as well as devices for measuring $p\text{CO}_2$ (Friederich et al., 1995) and pH (Martz et al., 2010). These tools have allowed the oceanographic community to make major research advancements.

A major focus of the Chemical Sensors Group at MBARI has been the development and dissemination of an in situ nitrate sensor. Nitrate is an essential plant nutrient, and its concentration exerts a

primary control on phytoplankton growth rates and biomass throughout much of the ocean (Falkowski et al., 1998). Annual and seasonal changes in nitrate concentration have been used to track net community production, which is defined as primary production minus respiration at all trophic levels (Wong et al., 1998, 2002; MacCreedy and Quay, 2001).

Development of an in situ chemical analyzer for nitrate has been enabled by advances in many technologies. The advent of flow injection analysis (FIA) in the late 1970s (Růžicka and Hansen, 1975) combined with technical advances in light-emitting diodes (LEDs) coupled to phototransistors (Betteridge et al., 1978) made it possible to develop a submersible chemical analyzer called SCANNER (Johnson et al., 1986a), which could be considered a "millifluidics" device. It was initially designed to measure hydrogen sulfide and silicate at hydrothermal vents (Johnson et al., 1986b, 1988), and was later adapted to measure nitrate concentrations in situ (Johnson et al., 1989). Prior to the development of FIA, automated chemical analyses of seawater required air bubbles in the sample stream to promote mixing while controlling dispersion (Hansen and Grasshoff, 1983; Johnson et al., 1986a), which made these analyses impossible to do underwater at depth (high pressure). Though SCANNER functioned at depth and achieved high-temporal-resolution measurements, it required chemical reagents, pumps, and tubing to propel the solutions, and, most critically, it had high power requirements that limited its utility in the field. Finding a low-power solution became an early focus.

Medical advances in the 1990s made osmotically powered pumps a commercially available option (Santus and Baker, 1995). These pumps require no external power, as flow is generated by the osmotic pressure created across a rigid

FACING PAGE. The many faces of the in situ ultraviolet spectrophotometer (ISUS). From top to bottom, left to right: drifter deployment, towfish deployment, autonomous underwater vehicle calibration, benthic flux chamber, remotely operated vehicle deployment, profiling rosette, Elkhorn slough cleaning, Elkhorn slough recovery, profiling float testing in Monterey Bay Aquarium Research Institute (MBARI) deepwater tank, profiling float deployment, and MBARI M1 mooring.

semipermeable membrane separating a saturated salt solution from one of lower salinity. Using this approach, a very low power “OSMOAnalyzer” was developed at MBARI to measure nitrate in situ (Jannasch et al., 1994). Low flow rates ($\mu\text{L h}^{-1}$) allowed the reaction manifold and conduits to be greatly reduced in size. This was, perhaps, the first “microfluidic” instrument used in oceanography. The OSMOAnalyzer was deployed on moorings in Bermuda (McNeil et al., 1999) and then Hawaii (Sakamoto et al., 2004). It was subsequently used to collect year-long measurements of iron in hydrothermal vent systems (Chapin et al., 2002). Although the OSMOAnalyzer did not use power-hungry mechanical pumps or pump tubes that wear out, it still relied on “wet chemistry” reactions with reagents and standards that deteriorate over time. Additionally, each fluidic connection, pump, or other component represents a single potential point of failure. Even with reasonably high reliability for each component in the reaction manifold, the large number of failure points resulted in low success rates, leading to the abandonment of these systems for measuring dissolved nitrate in situ.

Ultraviolet (UV) light absorption was another plausible approach for measuring nitrate concentrations in situ. The nitrate ion has a UV light absorption band near 200 nm due to a π to π^* electronic transition. Laboratory methods for the direct determination of nitrate using this absorption signal were proposed in the 1950s (Bastin et al., 1957), but their usefulness was limited by available technology. By the late 1990s, the idea of direct UV-absorption-based determination of nitrate had resurfaced in the oceanographic community, and methods using laboratory spectrophotometers were known (Collos et al., 1999). An instrument for in situ determination of nitrate at three wavelengths (later six) had been developed (Finch et al., 1998; Clayson, 2000). The difficulty with these methods was that the bromide and nitrate spectra overlap, so using a small number

of wavelengths made it numerically difficult to isolate nitrate. Three further technological advances solved this problem: (1) compact, low-power photodiode array spectrometers optimized for the UV; (2) stable, low power, continuous wave deuterium light sources; and (3) advances in fiber-optic technology and optical reflection probes that made it possible to make measurements in situ and collect the entire spectra to calculate nitrate concentrations. Johnson and Coletti (2002) developed and described the in situ ultraviolet spectrophotometer (ISUS), which measures nitrate in situ without reagents, standards, or pump tubes, all at low power. The energy requirement for a single ISUS scan is approximately 43 Joules per scan, so a 30 amp-hour battery pack (10.5V DC nominal) can power the instrument for six months taking triplicate scans once an hour. The technology was transferred to Satlantic Inc. the same year to make this development available to the greater scientific community.

ISUS deployments began on the MBARI M1 oceanographic mooring in October 2001 off the central California coast in Monterey Bay (Chavez et al., 2017a, in this issue), and have remained an integral part of the M1 sensor suite ever since. This paper describes results from these ISUS deployments—a high-resolution record that provides a window into ocean processes that cannot be achieved with conventional, shipboard measurements.

THE CASE FOR AUTONOMOUS IN SITU SENSORS AND PLATFORMS

Autonomous sensors that can operate in situ and for long time periods are needed to characterize temporal variability and to understand the role of nonsteady-state processes. Satellite images demonstrate that the ocean is highly dynamic. Yet, in most cases, chemical and biological data have only been obtained when shipboard personnel collect individual water samples for shipboard or laboratory analysis onshore. This process is prone to sample deterioration, and usually results

in a severe undersampling of the environment. The development of a low-power biologically relevant chemical sensor that could operate in situ for extended periods would increase the resolution needed to advance the understanding of biogeochemical cycles.

Platform development has also supported the deployment of instruments within observational networks. In addition to traditional platforms like ships, new platforms such as moorings (Chavez et al., 1997; Jannasch et al., 2008), autonomous underwater vehicles (Johnson and Needoba, 2008; Pennington et al., 2016), autonomous surface vehicles (Chavez et al., 2017b), and autonomous profiling floats (Johnson et al., 2013) have played increasingly important roles in oceanographic research.

MONTEREY BAY SETTING

The California Current (CC) is the eastern boundary of the North Pacific Gyre and flows southward at the surface from Oregon to Baja California. Monterey Bay is located at the eastern edge of the CC, at its midpoint in central California between 36.5°N and 37°N. The CC transports subarctic surface waters southward, while equatorial waters are transported poleward inshore and beneath the CC by the California Undercurrent (CUC), and, in winter, at the surface to 100 km offshore by the (Davidson) Inshore Countercurrent (IC; Collins, 2003). Monterey Bay is an open embayment, approximately 37 km along its north-south axis across the mouth and 19 km along its east-west axis.

Monterey Bay M1 Mooring

The M1 mooring lies in central Monterey Bay at 36.75°N, 122°W (Figure 1), along the axis of Monterey Submarine Canyon, midway between Santa Cruz and Monterey. The M1 mooring collects high-frequency (10 minutes) measurements of meteorological and oceanographic parameters (Chavez et al., 2017a, in this issue). Instructions and data are passed to and from shore via radio, and

data are plotted and distributed over the Internet in near-real time (Chavez et al., 1997). Although anchored in ~1,000 m of water, the mooring is less than an hour from shore, which encourages its use as an instrument test platform. The ISUS is deployed at 1 m depth.

METHODS

The ISUS Instrument

Ultraviolet light from a continuous wave, line-free lamp (Hereaus Fiberlight) passes through the solution to the probe's mirror and is reflected back through the sample solution to the probe's imaging optic (Johnson and Coletti, 2002). The intensities are measured using a Zeiss MMS spectrometer with holographic grating (256 wavelengths, ~200–400 nm; Johnson and Coletti, 2002; Figure 2). Nitrate concentration is deconvolved from the seawater absorption spectra measured directly in seawater from 217 nm to 240 nm. The spectra deconvolution assumes a three-component model, including bromide, nitrate, and a linear baseline (Johnson and Coletti, 2002). An improved algorithm corrects for the effect of temperature on the bromide signal (Sakamoto et al., 2009). Offsets and drifts due to biofouling or lamp drift were applied to the data based on discrete

nitrate samples collected during time-series cruises conducted by the MBARI Biological Oceanography Group (BOG).

Sensor performance was improved by developing a copper screen and Nitex mesh “Bioguard” to reduce biofouling (Figure 2). Although the copper reduced growth on the optical probe tip, principally by keeping the Nitex mesh clean, spectra are altered if copper is too close to the optics due to the formation of copper complexes in seawater. Ease of removal of the Bioguard had to be improved, as the probe tip would occasionally get sheared off during servicing by divers. Without the Bioguard, biofouling could occur in a matter of days. After implementation of the Bioguard, the longest ISUS deployment on M1 was 473 days, the length of the mooring deployment. Additionally, removing the lamp shutter, a mechanical point of failure for the system, was another MBARI modification that resulted in improved sensor performance.

RESULTS

Nitrate, Temperature, Salinity, Daily Upwelling Index

Figure 3b shows the 15-year hourly record of ISUS nitrate data from M1. Gaps in the nitrate data during the early years of deployment are primarily due to biofouling before development of the

copper Bioguard (Figure 2). After implementation of the Bioguard, data recovery was more robust; however, breaks in the record still occurred for various reasons, such as air bubbles trapped in the optical path, stuck lamp shutter, sheared off optical probe tip, and mooring communication lapses. There are 102,549 hourly nitrate measurements compared to 127,557 ISUS temperature measurements, equating to 80.4% data availability.

Figure 3a shows the daily upwelling index in units of $\text{m}^3 \text{s}^{-1}$ along 100 m of coastline, based on estimates of offshore Ekman transport driven by geostrophic wind stress (Bakun, 1973, 1975). These estimates of volume transport due to coastal upwelling were obtained from the NOAA Pacific Fisheries Environmental Laboratory upwelling index calculated at 36°N, 122°W.

Intense spring upwelling generally corresponds to periods of high nitrate, low temperature, and high salinity. Occasional periods of fresher seawater occurred during times of high runoff in winter (sharp lower salinity spikes; Figure 3d). However, the influence of terrestrially sourced and agriculturally influenced water on nitrate levels at the M1 mooring is poorly resolved when compared to the seasonal nitrate signal associated with coastal upwelling. Nitrate ($\mu\text{mol L}^{-1}$) and

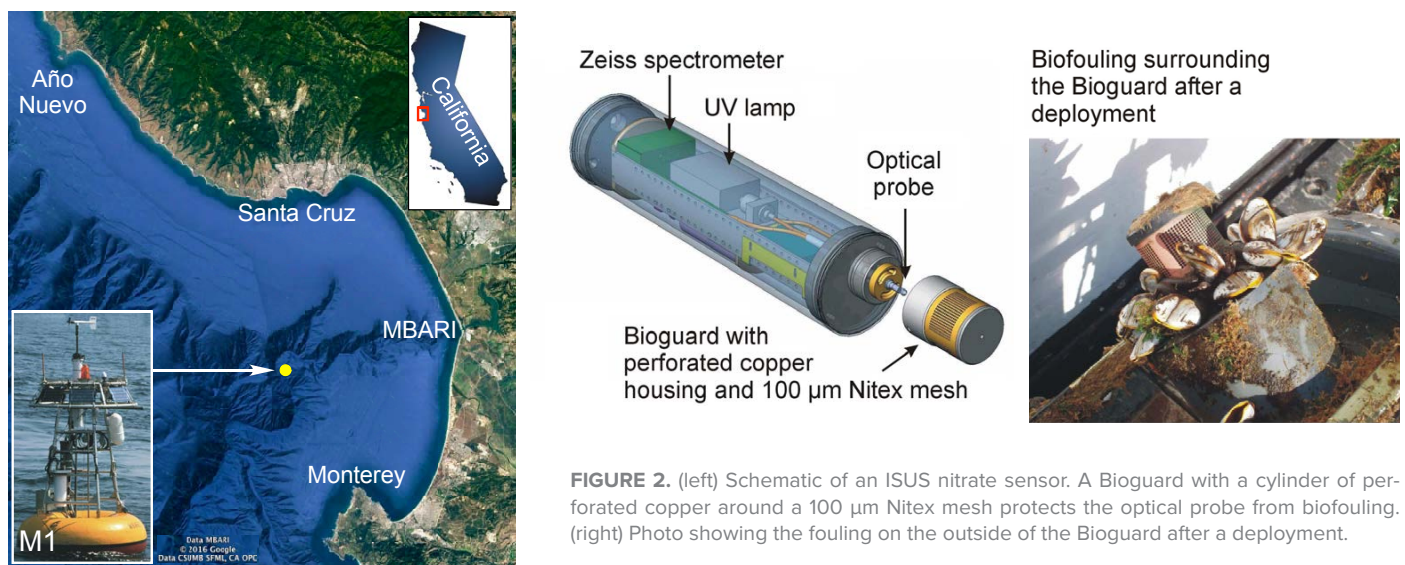


FIGURE 1. Location of MBARI and the M1 mooring.

FIGURE 2. (left) Schematic of an ISUS nitrate sensor. A Bioguard with a cylinder of perforated copper around a 100 μm Nitex mesh protects the optical probe from biofouling. (right) Photo showing the fouling on the outside of the Bioguard after a deployment.

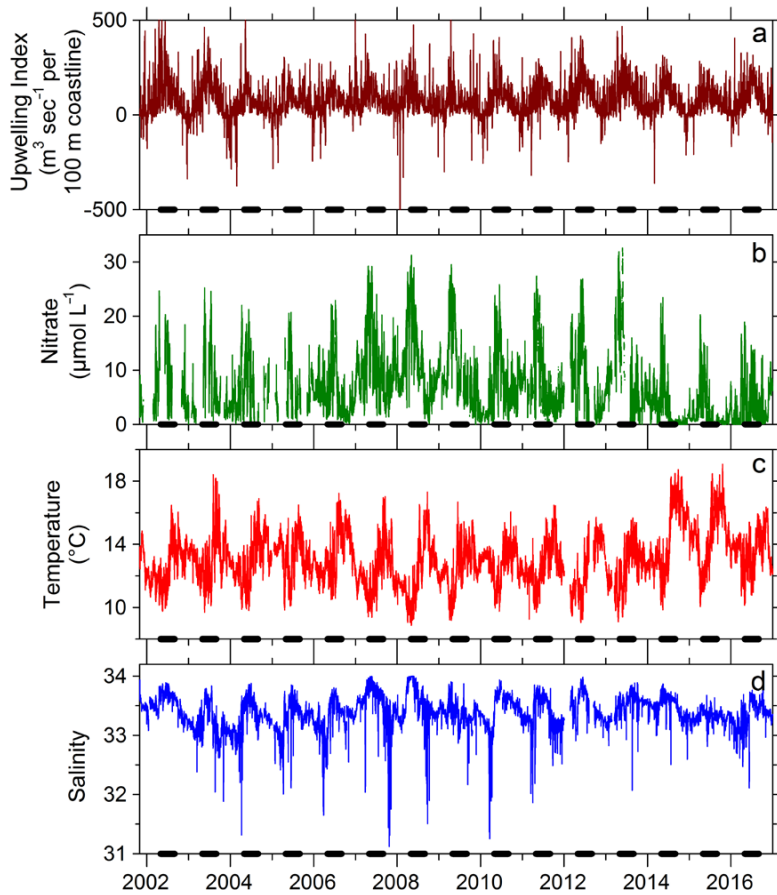


FIGURE 3. (a) Daily averaged upwelling index (units of $\text{m}^3 \text{sec}^{-1}$ along 100 m of coastline, upwelling conditions are positive). Hourly (b) nitrate, (c) temperature, and (d) salinity from the M1 mooring. The tic marks are January 1 of the year axis label. Black bands mark the May to August time period.

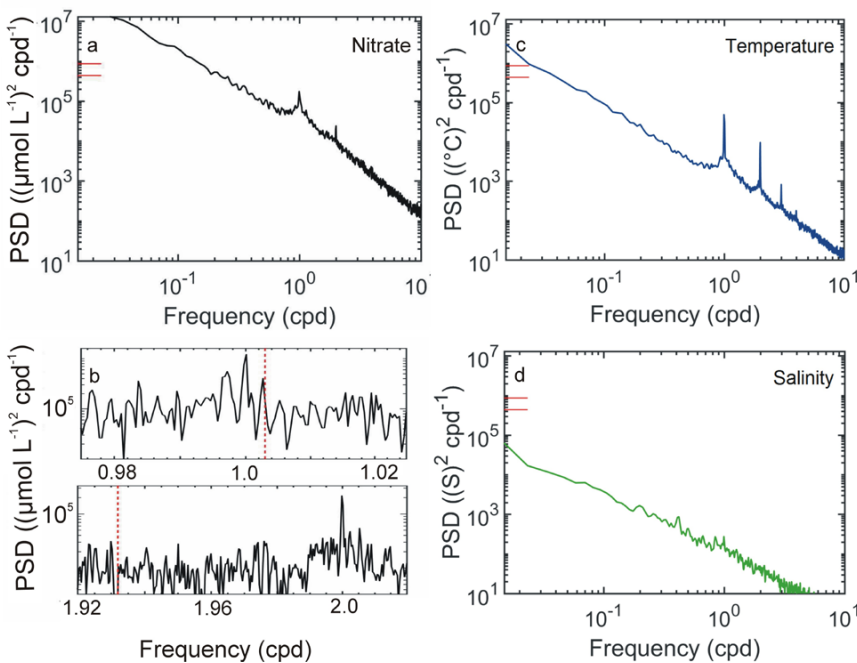


FIGURE 4. Power spectral density (PSD) estimates of (a) nitrate, (b) higher-resolution nitrate plots, (c) temperature, and (d) salinity data. The red solid lines show the 95% confidence interval. The two higher resolution nitrate plots (b) were generated using reduced averaging; red dashed lines represent the K1 and M2 tidal frequencies.

temperature ($^{\circ}\text{C}$) are inversely correlated ($\text{NO}_3^- = -2.82 (\pm 0.007) \times \text{temp} + 43.59 (\pm 0.01)$, $r^2 = 0.59$, 95% CI).

Time Series Data Analysis

The high temporal resolution (hourly) of the more than 15 years of data enabled the application of time-series analysis methods to examine the data in terms of its frequency content. Mooring data were uniformly gridded on an hourly basis prior to the time-series analysis. Gaps in the gridded data were filled by linear interpolation between the data points bracketing the gaps. There were 1,101 independent data gaps; the largest gap spanned 1,976 data points, and 81% of the gaps spanned fewer than six data points. In total, there were 30,631 interpolated data points out of 133,180 total (23%). Power spectral density (PSD) plots were then generated with Welch's averaged modified periodogram method using a Hamming window (Welch, 1967; Harris, 1978) to identify periodicities in the data. A window size of 2^{11} samples was used with 50% overlap between segments to identify significant peaks in each power spectrum (Figure 4a,c,d). Higher resolution PSD plots were then generated to further investigate the frequency characteristics associated with spectral peaks (Figure 4b). These plots were generated in the same way, but with 2^{16} samples per segment with 50% overlap between segments (reduced averaging), which gives a PSD frequency range from 0 to 12 cycles per day with a frequency resolution of 0.00037 cycles per day (Figure 4b). Generating PSDs with high-frequency resolution was essential for separating diel biological cycles from closely spaced tidal harmonics with similar frequencies.

To further hone in on high-frequency signals associated with diel biological processes, low-frequency variability in the data due to physical processes such as upwelling events was removed by applying a 256th order finite impulse response (FIR) filter designed with a pass band starting at 0.7 cycles per day (34.3-hour

period) and stopband attenuation of 60 db. The time delay introduced by the group delay of the filter was removed by eliminating the first $(N-1)/2$ data points from the filtered data set, where N = the filter order (256). The amplitudes of the diel changes in nitrate concentration were then obtained from this filtered data set as discussed below.

Daily Nitrate Uptake Signal

As described previously, Figure 4 shows the PSD plots of the hourly nitrate, temperature, and salinity data. The PSD characterizes the frequency content of the data and reveals any significant periodicities. Distinct peaks at exactly one cycle per day (10^0 cpd) can be seen in the nitrate and temperature data but not in the salinity data. The strong peaks at 2 cpd and 3 cpd in the temperature periodogram are harmonics of the 1 cpd signal. These daily peaks are well resolved from the lunar tidal K1 constituent at 1.003 cpd and the dominant M2 semidiurnal tidal component at 1.932 cpd (Figure 4b). The daily signal in temperature is due to insolation during the day and cooling during the night. The absence of a significant 1 cpd salinity signal confirms that the nitrate diurnal signals are not due to other daily physical processes that could produce advective fluxes.

Johnson et al. (2006) and Johnson (2010) reported the 1 cpd signal in nitrate concentrations. Nitrate is taken up by phytoplankton during growth in the daylight (“drawdown”), overcoming resupply processes. Those studies and others using this methodology (Collins et al., 2013; Martz et al., 2014) emphasize this diel signal by passing the data through a high-pass filter, similar to that used here, so that lower-frequency processes are removed while the daily variability remains. The high-frequency nitrate measurements provide a basis for these time-series analyses, enabling estimation of phytoplankton daily drawdown (nitrate uptake).

Figure 5 shows the timing of the daily minimum (trough) and maximum (peak)

values of the high-pass-filtered nitrate. Daily minima are centered at 1700 hours local time, as expected, because phytoplankton take up or “assimilate” nitrate largely during daylight hours, especially in nutrient replete environments such as Monterey Bay (Cochlan et al., 1991; Kudela et al., 1997). Dark assimilation of nitrate is important under nutrient-limited conditions for some phytoplankton that assimilate nitrate by vertical migration, and this may also occur in Monterey Bay (Ryan et al., 2010); however, dark assimilation would likely impact nitrate at depth and not at the surface. The timing of the nitrate maxima in a given 24-hour period reflects the timing of the daily nitrate minima in the afternoon, with a fairly uniform distribution during the rest of the day. It is unclear why the noon to 1 pm and 10 pm to 11 pm periods have a slightly higher number of peaks. There is no strong diel driver that would regulate the maximum to a particular period of the day, so having a fairly uniform distribution would be expected outside times of drawdown.

The 34-hour high-pass-filtered data were used to generate daily nitrate uptake values, calculated by finding the minimum value between 12 pm and 8 pm each day and subtracting it from the maximum value occurring between 12 am and 12 pm for that day. Days within ± 1 day of signal padding were rejected, resulting in $n = 4,865$ days out of 5,542 days. Concurrent salinity measurements were used to further filter the data set by rejecting data points where the salinity difference between the maxima and minima was greater than 0.125. This resulted in $n = 3,896$ days for which daily nitrate uptake values were used for further analysis. Large differences in salinities were taken to reflect influence of advective water mass changes, rather than drawdown, on the delta nitrate values.

Seasonal Variability

The seasonal variability of Monterey Bay is described elsewhere (Pennington and Chavez, 2000; Chavez et al., 2017a,

in this issue), along with annual cycles (Pennington et al., 2010) and non-seasonal anomalies with Pacific basin-scale climate indices (Pennington and Chavez, 2017). A brief description based on hourly nitrate, temperature, and salinity and daily upwelling index and nitrate uptake data follows to provide oceanographic context. To look at seasonal variability, a monthly climatology was created from the data to represent an “average year” for each property (Figure 6). Confidence intervals (95%) of the mean were calculated using a correction factor (Bence, 1995) for the autocorrelation of the data. This average year was based only on 2001–2013 data, as the data from 2014–2016 were so anomalous that they skewed the average year results. This anomalous warm period will be discussed separately.

In the early spring of an average year, as upwelling-favorable winds increase, saltier, colder, higher nitrate upwelled water is measured at M1. The upwelling season is characterized by intense periods of northwesterly winds that drive the vertical transport of this relatively cold, salty, high-nutrient water to the surface (Ramp et al., 2005). An upwelling center north of

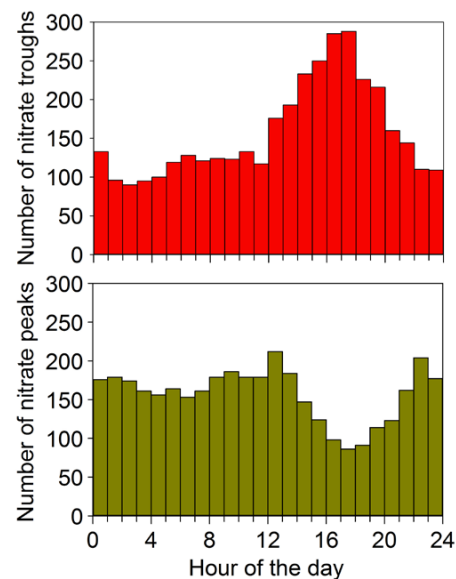


FIGURE 5. The number of daily maximum (peak) and minimum (trough) values in the 34-hour high-pass-filtered nitrate data during each local hour of the day. Data within one day of signal padding were excluded.

Monterey Bay near Pt. Año Nuevo is the main source of recently upwelled water in Monterey Bay (Rosenfeld et al., 1994). Daily nitrate uptake starts to increase significantly in March along with increases in nitrate concentrations. This early upwelling brings dissolvable iron to the surface water from the fluff layer on the shelf (Elrod et al., 2008). Shoaling of the isotherms brings water that was in contact with the shelf to the surface, resulting in a pulse of iron that drops over the next few months even as nitrate concentrations continue to increase (Elrod et al., 2008). During this time period, diatoms dominate as primary productivity in the bay starts to ramp up (Chavez et al., 2017a, in this issue). The means of the coldest temperatures, highest nitrate, and highest nitrate uptake occur in May, while the means of the salinities and upwelling index continue to increase, reaching their peaks in June.

As summer progresses, the prevailing northwesterly winds weaken (“relaxation” from upwelling), upwelling slows and stratification intensifies, and the offshore warm surface waters move onshore (Rosenfeld et al., 1994). Local surface heating in the bay also occurs (Ramp et al., 2005). During relaxation, more uniform conditions prevail, with lower salinities and warmer temperatures throughout the bay. The monthly mean

surface nitrate, salinity, and upwelling-favorable winds decrease. The highest mean of the surface temperatures occurs in August–September. This season coincides with the prevalence of picophytoplankton and dinoflagellates in the bay (Chavez et al., 2017a, in this issue).

Toward the end of the fall months, winter storms begin, with episodes of strong southerly winds. The mixed layer deepens due to intensified storms and mixing, and surface waters tend to be warmer, fresher, and less nutrient-rich relative to other times of the year (Pennington and Chavez, 2000). The lowest mean nitrate concentrations occur during September–October, with average nitrate uptake of $1.2 \mu\text{mol L}^{-1} \text{day}^{-1}$. During the November–February time period, the mean of the nitrate concentrations increases up to $6.2 \mu\text{mol L}^{-1}$. The nitrate uptake mean is lowest during January–February, averaging $0.9 \mu\text{mol L}^{-1} \text{day}^{-1}$.

Episodes of upwelling and wind relaxations and reversals that produce downwelling occur throughout the year. The highest frequency and duration of upwelling events occur during the spring and summer upwelling season. Sustained winds of at least 10 m s^{-1} are needed for about a week before the upwelling filament will spread significantly southward to the M1 mooring (Ramp et al., 2005).

The average year variability agrees well

with accepted descriptions of seasonal variability in Monterey Bay (Pennington and Chavez, 2000; Pennington et al., 2010; Chavez et al., 2017a, in this issue). The more than 15-year high-temporal-resolution data add confidence to our understanding of the current oceanographic regime of Monterey Bay.

Interannual Variability

In addition to reinforcing our understanding of seasonal cycles and associated oceanographic responses in Monterey Bay, the 15+ year time-series record at M1 also provides insight into interannual variability, spanning multiple El Niño/La Niña events and capturing an anomalously warm year that preceded a historically strong El Niño. To emphasize interannual variability, the previously described monthly “average” year data were subtracted from monthly binned data to plot monthly anomalies along with the Oceanic Niño Index (ONI: blue La Niña conditions, red El Niño conditions in Figure 7). In general, La Niña is associated with saltier, colder, higher nitrate and higher nitrate uptake waters, while El Niño is associated with fresher, warmer, lower nitrate and lower nitrate uptake waters, but the interplay of the timing and duration of upwelling-favorable winds and ONI also affects nitrate uptake.

The most distinct anomaly period is 2014–2016 (Figure 7), with anomalies over three very warm years. Strong positive temperature anomalies developed in the Northeast Pacific Ocean during the winter of 2013–2014 (Bond et al., 2015). This anomalous warm water became referred to as “the Blob” in the general press and was linked to unusually high sea level pressure that resulted in lower than normal rates of heat loss from the ocean to the atmosphere and relatively weak cold advection in the upper ocean (Bond et al., 2015). The positive temperature anomaly started at M1 at the beginning of 2014 during a period of weak La Niña. This anomalous low-nutrient warm water was associated with the

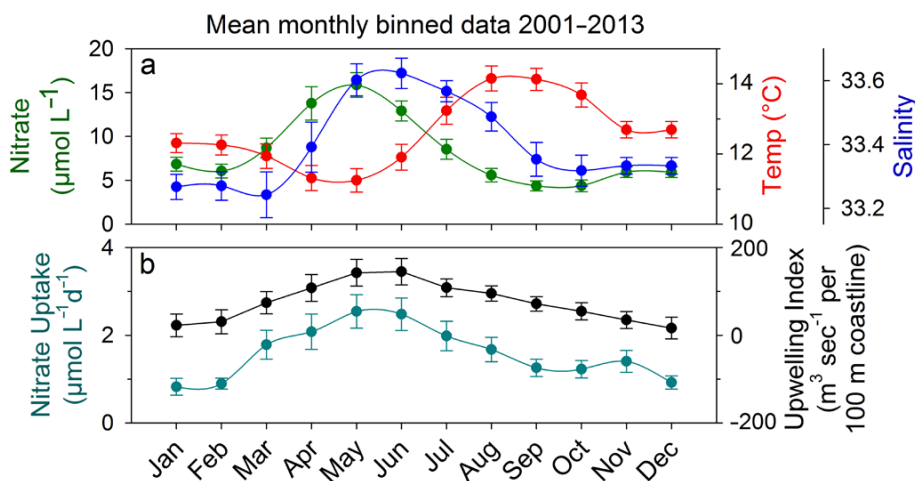


FIGURE 6. Monthly binned data from 2001 to 2013. (a) Nitrate (green), temperature (red), and salinity (blue). (b) Nitrate uptake (teal) and upwelling index (black). The mean and the 95% CI (confidence interval) of the mean calculated according to Bence (1995). Upwelling-favorable winds are positive.

largest recorded outbreak of a coastwide toxic algal bloom that closed fisheries and propagated up the food chain to ultimately affect the health of marine mammals (McCabe et al., 2016). Low-nutrient, warm, low-productivity water persisted through 2016 during a period that brought a historically strong El Niño beginning in late 2014. The 2015–2016 El Niño was the strongest since the 1997–1998 event. Outbreaks of toxic algal blooms, fisheries closures, and marine mammal mortality continued along the West Coast (Ryan et al., 2017) during the winter of 2016–2017, as well as historically high levels of precipitation (Figure 7). These results further document previously recorded interannual variability (Pennington and Chavez, 2000; Pennington et al., 2010; Chavez et al., 2017a, in this issue).

Daily Nitrate Uptake and ¹⁴C Primary Productivity

The hourly sampling rate of the ISUS enabled calculations of daily nitrate uptake as described previously. The primary productivity as measured by ¹⁴C uptake in 24-hour bottle incubations (Pennington and Chavez, 2000, 2017b; Chavez et al., 2017a, in this issue) and the nitrate uptake measured on the same day are plotted in Figure 8. The daily nitrate uptake values are converted to C units in mg m⁻³ using the Redfield ratio (nitrate uptake in μmol L⁻¹ day⁻¹ × 6.6 μmol C/μmol N × 12 μg C/μmol C × mg C/1,000 μg C × 1,000 L m⁻³). The solid line is the Model II regression equation (R = 0.35):

$$\text{nitrate uptake} = 0.48 (\pm 0.04) \times \\ {}^{14}\text{C primary production} + 13.2 (\pm 13.1).$$

Nitrate uptake values during the daytime represent the difference between (1) nitrate consumption by photosynthesis, and (2) the resupply of nitrate from either upward diffusive or lateral advective fluxes. The contribution of nitrate via nitrification (Smith et al., 2014) is assumed to be of secondary importance relative to advective fluxes in Monterey Bay surface waters. The ¹⁴C uptake in incubation bottles during daylight approximates net primary production (Marra, 2009). The 24-hour ¹⁴C incubations used for this data can produce uptake values lower than net primary production, as they include significant respiration during the dark, often ~20% at the surface in Monterey Bay (Pennington et al., 2016). In addition, for 24-hour ¹⁴C incubations, samples spiked at dusk will be biased high compared to samples spiked at dawn (Pennington et al., 2016). Given those caveats, the ¹⁴C incubations will be used as measures of net primary production, equivalent to “total production” (Manning et al., 2017).

Primary production can be further partitioned into “new” production based on nitrate uptake and “regenerated” production based on ammonium and

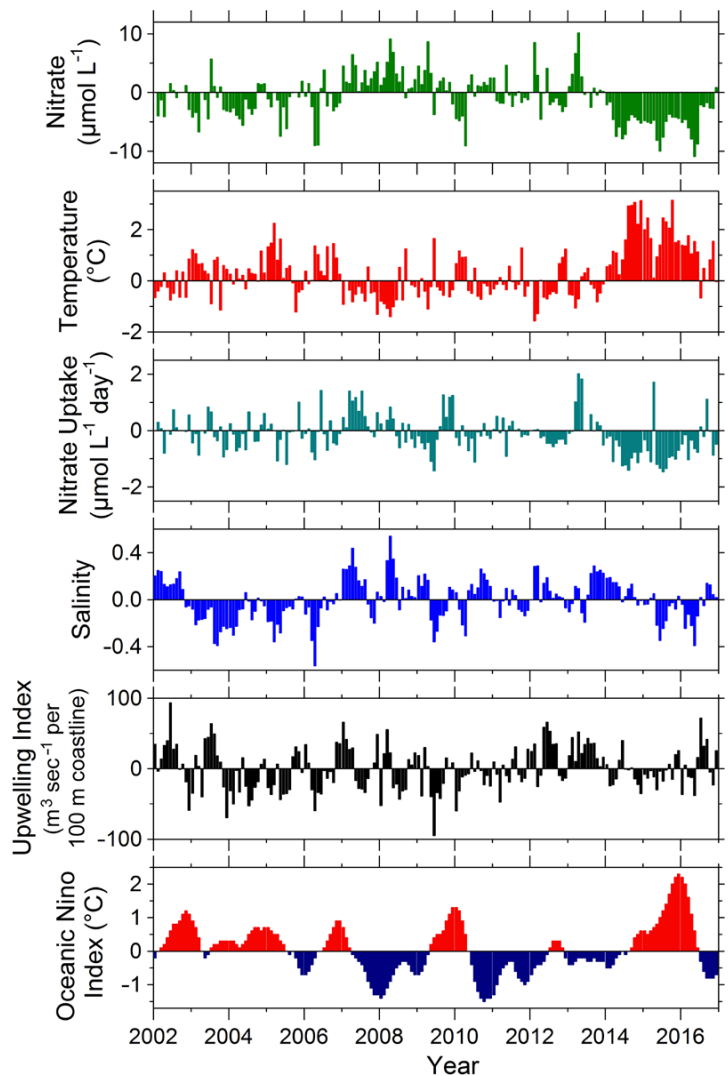


FIGURE 7. Top to bottom: M1 nitrate, temperature, nitrate uptake, salinity, and upwelling index anomalies generated by subtracting the monthly “average year” calculated from 2001 through 2013 and subtracted from monthly binned data. The bottom panel is the Oceanic Niño Index (from <http://www.pfeg.noaa.gov>), which is one measure of the El Niño–Southern Oscillation.

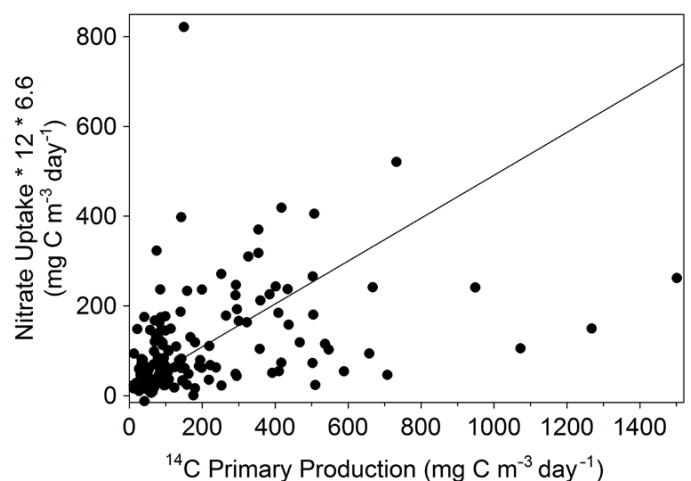


FIGURE 8. Daily nitrate uptake converted to C units by using the Redfield ratio plotted versus the ¹⁴C primary production measured in 24-hour bottle incubations. The solid line is the Model II regression equation.

organic nitrogen (Dugdale and Goering, 1967). The f-ratio is the ratio of nitrate-based new production to total production (Eppley and Peterson, 1979). If the nitrate uptake is considered a proxy for new production and ^{14}C primary production a measure of total production, then the slope of Figure 8 gives an f-ratio of 0.48 for these individually matched samples. The scatter in Figure 8 may result from comparing nitrate uptake measured over a complete day with ^{14}C primary production in a small sample collected at an instant in time. Pennington et al. (2010) calculated an annual f-ratio in Monterey Bay of 0.49, Olivieri and Chavez (1996) calculated 0.84 based on modeling results, and enclosure experiments in Monterey Bay measured f-ratio values ranging between 0.35 and 0.80 (Kudela and Dugdale, 2000). In a comparison of in situ and incubation-based methods in Monterey Bay, Manning et al. (2017) reported ef-ratios (ef-ratio = new production/net primary production = net community production/net primary production) that ranged from 0.17 to 0.84, depending on the analytical method used and upwelling conditions.

To smooth the variability in the data, all the nitrate uptake values from 2001–2016 were converted to C units as before

by using the Redfield ratio and ^{14}C primary productivity values were binned by month; the monthly mean and the 90% confidence interval (Bence, 1995) are plotted in Figure 9a. Months that have significantly different medians (Mann-Whitney Rank Sum test; $P < 0.05$) for the nitrate uptake and ^{14}C -based primary production estimates are marked with an asterisk (Figure 9a). The confidence intervals for the ^{14}C data are based on a much smaller number of observations than are available for the nitrate uptake data and have correspondingly larger values. The medians for the winter months of November–February are statistically similar, with low values of both nitrate uptake and ^{14}C primary production. May has the highest nitrate uptake, but the ^{14}C primary production is only slightly higher, and the median is not significantly different. The other upwelling months have statistically significantly higher medians of ^{14}C primary production than the nitrate uptake.

Figure 9b plots the mean monthly values of nitrate uptake converted to C divided by ^{14}C primary production (f-ratio) versus ^{14}C primary production. For November–February and May, the ratio of the nitrate uptake to ^{14}C primary productivity (f-ratio) (Figure 8c,

red circles and a blue circle) ranges from 0.72 to 1.2 (mean = 0.86 ± 0.2). In March, April, June, July, August, September, and October, the nitrate uptake median value is statistically lower than the ^{14}C value ($P < 0.001$), and these months are plotted in Figure 9b as green circles with f-ratios ranging from 0.36 to 0.51 (mean = 0.47 ± 0.05). Eppley and Peterson (1979) plots of f-ratios follow a hyperbolic curve from low values in low-productivity regions up to 0.5 in Peru upwelling waters; however, the lowest f-ratios calculated here are during the high-productivity months. The shape of the curve based on Olivieri and Chavez (2000) modeled f-ratio values also changed throughout the year; however, their highest values were during the spring/summer months (0.8–0.9), with lower values during the late fall/winter period, as their regenerated nutrient uptake rate was relatively low and constant throughout the year but their nitrate uptake increased as a function of upwelling. In our data, the nitrate uptake does increase as a function of upwelling and higher nutrient concentrations; the ^{14}C primary production data also exhibit this relationship, but the relative increase is much higher, which drives the f-ratio lower by having a larger denominator.

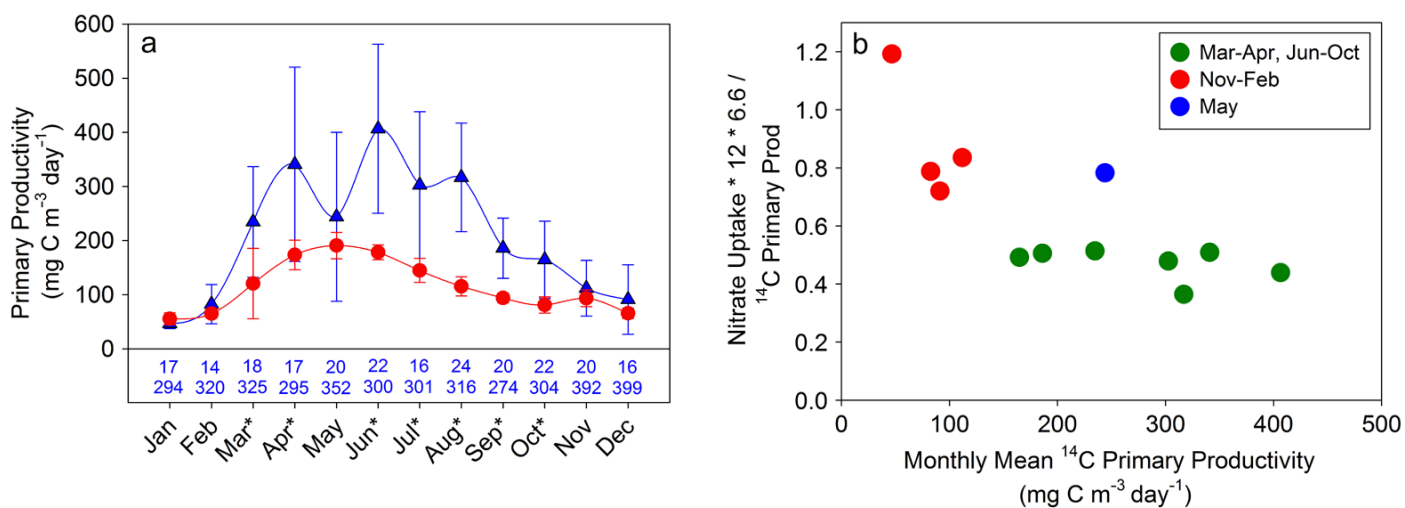


FIGURE 9. (a) Monthly mean daily nitrate uptake values (red circle) converted to C and ^{14}C primary productivity values (blue triangles) binned by month. The mean and 90% confidence intervals are calculated according to Bence (1995). The number of observations based on daily nitrate uptake (red) and ^{14}C primary productivity (blue) are listed at the bottom of the chart. * indicates months with significantly different medians. (b) The monthly mean nitrate uptake converted to C divided by ^{14}C primary production (f-ratio) versus ^{14}C primary production.

In the winter months when ^{14}C primary productivity and nitrate uptake are both low, the ratio approaches one.

The e-ratio is the ratio of export production to total production, and when averaged over an appropriate temporal and spatial scale, the e-ratio and f-ratio should be equivalent (new production = export production, if there is no change in biomass). This classic relationship between export production and primary production reported by Eppley and Peterson (1979) would suggest that nitrate-based production estimated from sensor data and primary production from ^{14}C data should be most similar in the spring and summer months, as there are unlikely to be other, significant sources of nitrogen to support primary production. However, an inverse relationship between carbon export and productivity, relative to Eppley and Peterson (1979), has been noted before in Monterey Bay (Pilskaln et al., 1996; Oliveri and Chavez, 2000; Pennington and Chavez, 2010), as well as other environments (Maiti et al., 2013; Le Moigne 2016). In these studies, the e-ratio values are inversely proportional to primary production, with the highest values during the low-productivity months. Explanations for the minimal e-ratios during upwelling months in

Monterey Bay have included enhanced offshore transport during upwelling months (spatial decoupling of the locations of primary production and carbon export in Monterey Bay) and secondarily by an increase in the abundance of water column detritus feeders during the upwelling season (Pilskaln et al., 1996; Olivieri et al., 2000). Zooplankton grazing has also been hypothesized to explain an inverse export production to primary production relationship in the Southern Ocean (Le Moigne et al., 2016). If ^{14}C primary production values in Monterey Bay are relatively higher during the upwelling season due to less zooplankton grazing, especially at night, then our observations make sense.

The daily nitrate uptake and the daily upwelling index values (2001–2016) were binned into the 12 months, and the means and 90% CI are plotted in Figure 10a with December–February (red squares), March–August (green squares), and September–November (blue squares) data. The solid line is the Model II regression equation of the mean monthly nitrate uptake versus mean monthly upwelling index ($R = 0.94$):

$$\text{nitrate uptake} = 0.013 (\pm 0.001) \times \text{upwelling index} + 0.47 (\pm 0.1).$$

The mean monthly nitrate uptake shows high correspondence to the mean monthly upwelling index, with the highest values occurring during the upwelling season (March–August). Reduced mean monthly nitrate uptake values are observed through the fall (September–November), with lowest values occurring during winter (December–February).

The daily nitrate uptake values and the nitrate concentrations for 2001–2016 were binned into the 12 months, and the means and 90% CI are plotted in Figure 10b with the same color scheme as in Figure 10a. The Model II equation of the mean monthly nitrate uptake versus the mean nitrate concentration ($R = 0.87$) is

$$\text{nitrate uptake} = 0.17 (\pm 0.02) \times \text{nitrate} + 0.26 (\pm 0.2).$$

The December–February (red squares) data during this time period are a minima in accordance with Pennington and Chavez (2000). The reduced number of daylight hours and increased depth of the mixed layer reduce the nitrate uptake below what would be simply expected based on the nitrate concentration.

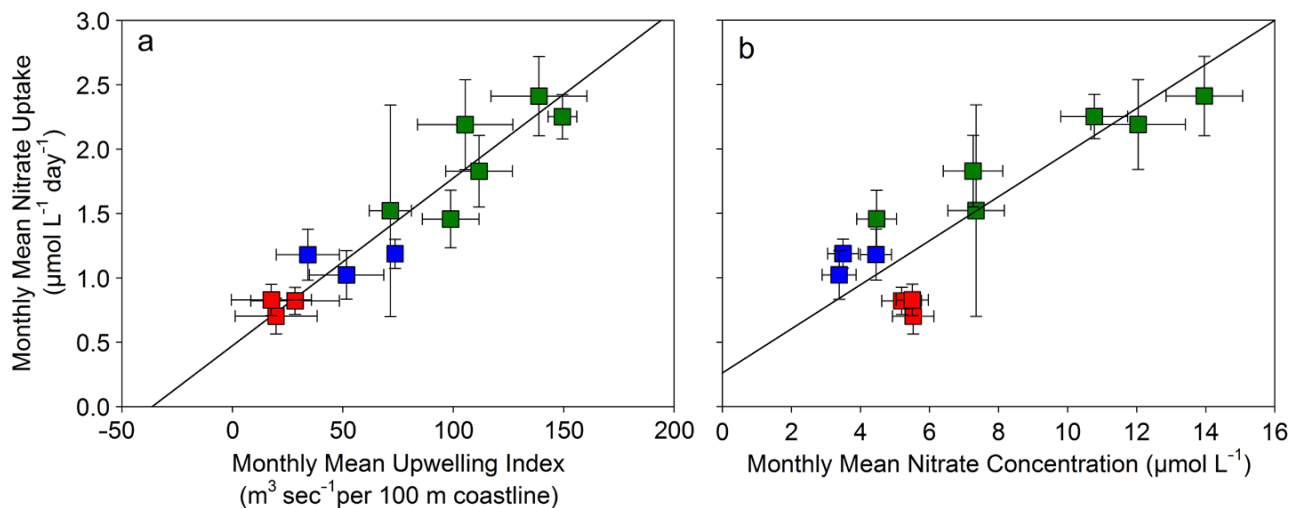


FIGURE 10. (a) The 2001–2016 monthly mean daily nitrate uptake versus monthly binned upwelling index, and (b) versus monthly binned nitrate concentration. The solid line is the Model II regression equation. The mean for December–February (red squares), March–August (green squares), and September–November (blue squares) and the 90% CI of the mean are shown as error bars.

SUMMARY

The development of a low-power nitrate sensor that can operate remotely for long periods without “wet” chemistry, as well as the transfer of this technology, has enabled its use on a variety of platforms. Ready access to MBARI moorings and concurrent time-series ship work provided a testbed that permitted refinement of ISUS so that it can be remotely deployed for years and integrated into globally distributed biogeochemical sensor networks.

The effects of seasonal variability and interannual events, such as La Niña and El Niño, and anomalous water masses are captured and illustrate the importance of upwelling frequency and nutrient availability to the productivity of Monterey Bay. The more than 15 year record con-

FUTURE VISION

Advances in science can indeed come from advances in technology. Being able to determine dissolved nitrate with high temporal resolution without power-hungry pumps or deteriorating reagents and standards has spread to uses that were not envisioned during the initial stages of development. For example, there is now widespread use of UV optical instruments for measuring nitrate in freshwater studies. Diel variation in nitrate concentrations has been studied in rivers by collecting high-frequency measurements with an ISUS (Pellerin et al., 2009) and other submersible ultraviolet analyzers such as the submersible ultraviolet nitrate analyzer (SUNA; Burns et al., 2016; Hensley and Cohen, 2016) and the hyperspectral UV-spectrometer

University of California Cooperative Extension in nearby agricultural fields in a feasibility study of the use of ISUS to provide a control feedback loop in an agricultural wood chip denitrification bioreactor (Hartz et al., 2017). Available real-time nitrate data were used to optimize the application of carbon enrichment to promote complete nitrate removal in an agricultural field tile drainage with minimal adverse environmental effects (Hartz et al., 2017).

In the future, increasing data collection spatial resolution through deployments on other autonomous platforms such as surface wave gliders, autonomous underwater vehicles, and autonomous profiling floats will serve to further expand potential research capabilities. Both ISUS (Johnson and Needoba, 2008; Ryan et al., 2010; Harvey et al., 2012; Zhang et al., 2015; Fischer et al., 2017) and SUNA (Wulff, 2016; Karstensen et al., 2017) nitrate sensors have been successfully deployed on autonomous underwater vehicles. In the future, incorporation of UV optical nitrate sensors along with pH and $p\text{CO}_2$ sensors on surface wave gliders (Chavez et al., 2017b) will provide quantitative data on the coupling of the carbon and nutrient cycles.

The integration of optical nitrate sensors and pH sensors for use in biogeochemical studies has already been implemented on certain platforms. For the last 10 years, optical nitrate sensors have been deployed on profiling floats throughout the world ocean (Johnson et al., 2010, 2013; D’Ortenzio et al., 2014; Pasqueron de Fommervault et al., 2015; Johnson and Claustre, 2016; Plant et al., 2016). A current collaboration in a program deploying optical nitrate sensors on profiling floats around the Southern Ocean (Johnson et al., 2013, 2017a,b) incorporates the recent development of a low-power, deep-sea Durafet for measuring pH (Johnson et al., 2016). These Biogeochemical-Argo floats autonomously profile from 1,600 m depth to the surface every 10 days and can last for 6.5 years, measuring nitrate, pH, oxygen, and bio-optics (Johnson

“ An expanding number of ultraviolet optical nitrate sensor deployments on moorings and autonomous platforms such as profiling floats will provide ever-broadening coverage of the world ocean, resulting in enhanced spatial and temporal resolution of nitrate measurements and, ultimately, improved insight into the dynamics of nitrogen cycling and phytoplankton ecology throughout a changing global ocean. ”

firms previous studies with increased confidence from the dense data set.

The hourly record of nitrate concentrations on the M1 mooring allows estimation of nitrate uptake with the use of time-series analysis methods. Calculation of a proxy for new production using a low-power remote sensor that can be deployed for years without using wet chemistry methods is a powerful tool.

TRIOS ProPS-UV sensor (Aubert and Breuer, 2016; Rode et al., 2016). ISUS was also used to monitor nitrate and bisulfide in a mercury-polluted, eutrophic lake in New York after implementation of nitrification treatment, and it plays an important role in rehabilitation programs for the lake (Prestigiacomo et al., 2009).

Another use not originally envisioned involved collaboration with the

et al., 2017a). The Southern Ocean is a very difficult region to study because of its remote location, inhospitable weather, and rough seas, yet it is an area of critical importance with regard to understanding the ocean's capacity to take up excess atmospheric CO₂ contributed by anthropogenic inputs. Deploying around 200 profiling floats over a six-year period in this remote, inhospitable region will yield a spatially dense, long-term data set that will document the region's influence on global climate and support the modeling of biogeochemical fluxes. The proposed deployment of a global array of Biogeochemical-Argo floats will enable us to monitor the ocean and work cooperatively with other nations in a new way.

A system for managing profiling float data is critical to their use by the community at large. The requirement of having Biogeochemical-Argo data openly available in near-real time on the web has forced improvements in automating quality control and post-processing of the data. Building upon the framework of data recovery and dissemination developed for MBARI's coastal moorings, Biogeochemical-Argo float data are available through a user-friendly interface to the entire scientific community. 

REFERENCES

- Aubert, A.H., and L. Breuer. 2016. New seasonal shift in in-stream diurnal nitrate cycles identified by mining high-frequency data. *PLoS ONE* 11(4):e0153138, <https://doi.org/10.1371/journal.pone.0153138>.
- Bakun, A. 1973. *Coastal Upwelling Indices, West Coast of North America, 1946–1971*. US Department of Commerce, NOAA Technical Report NMFS-SSRF-671, 103 pp.
- Bakun, A. 1975. *Daily and Weekly Upwelling Indices, West Coast of North America, 1967–1973*. US Department of Commerce, NOAA Technical Report NMFS-SSRF-693, 114 pp.
- Bastin, R., R. Weberling, and F. Palilla. 1957. Ultraviolet spectrophotometric determination of nitrate... Application to analysis of alkaline earth carbonates. *Analytical Chemistry* 29:1795–1797, <https://doi.org/10.1021/ac60132a038>.
- Bence, J.R. 1995. Analysis of short time series: Correcting for autocorrelation. *Ecology* 76(2):628–639, <https://doi.org/10.2307/1941218>.
- Betteridge, D., E.L. Dagless, B. Fields, and N.F. Graves. 1978. A highly sensitive flow-through phototransducer for unsegmented continuous-flow analysis demonstrating high-speed spectrophotometry at the parts per 10⁹ level and a new method of refractometric determinations. *Analyst* 1230:897–908, <https://doi.org/10.1039/AN9780300897>.
- Bond, N.A., M.F. Cronin, H. Freeland, and N. Mantua. 2015. Causes and impacts of the 2014 warm anomaly in the NE Pacific. *Geophysical Research Letters* 42:3,414–3,420, <https://doi.org/10.1002/2015GL063306>.
- Burns, D.A., M.P. Miller, B.A. Pellersin, and P.D. Capel. 2016. Patterns of diel variation in nitrate concentrations in the Potomac River. *Freshwater Science* 35:1,117–1,132, <https://doi.org/10.1086/688777>.
- Chapin, T.P., H.W. Jannasch, and K.S. Johnson. 2002. In situ osmotic analyzer for the year-long continuous determination of Fe in hydrothermal systems. *Analytica Chimica Acta* 463:265–274, [https://doi.org/10.1016/S0003-2670\(02\)00423-3](https://doi.org/10.1016/S0003-2670(02)00423-3).
- Chavez, F.P., J.T. Pennington, R.A. Herliem, H.W. Jannasch, G. Thurmond, and G.E. Friederich. 1997. Moorings and drifters for real-time interdisciplinary oceanography. *Journal of Atmospheric and Oceanic Technology* 14:1,199–1,211, [https://doi.org/10.1175/1520-0426\(1997\)014<1199:MADFRT>2.0.CO;2](https://doi.org/10.1175/1520-0426(1997)014<1199:MADFRT>2.0.CO;2).
- Chavez, F.P., J.T. Pennington, R.P. Michisaki, M. Blum, G.M. Chavez, J. Friederich, B. Jones, R. Herliem, B. Kieft, B. Hobson, and others. 2017. Climate variability and change: Response of a coastal ocean ecosystem. *Oceanography* 30(4):128–145, <https://doi.org/10.5670/oceanog.2017.429>.
- Chavez, F.P., J. Sevadjian, C. Wahl, J. Friederich, and G.E. Friederich. 2017b. Measurements of pCO₂ and pH from an autonomous surface vehicle in a coastal upwelling system. *Deep Sea Research Part II*, <https://doi.org/10.1016/j.dsr2.2017.01.001>.
- Clayton, C.H. 2000. Sensing of nitrate concentration by UV absorption spectrophotometry. Pp. 107–121 in *Chemical Sensors in Oceanography*. M.S. Varney, ed., Gordon and Breach.
- Cochlan, W.P., P.J. Harrison, and K.L. Denman. 1991. Diel periodicity of nitrogen uptake by marine phytoplankton in nitrate-rich environments. *Limnology and Oceanography* 36:1,689–1,700, <https://doi.org/10.4319/lm.1991.36.8.1689>.
- Collins, C.A., J.T. Pennington, C.G. Castro, T.A. Rago, and F.P. Chavez. 2003. The California Current System off Monterey, California: Physical and biological coupling. *Deep Sea Research Part II* 50:2,389–2,404, [https://doi.org/10.1016/S0967-0645\(03\)00134-6](https://doi.org/10.1016/S0967-0645(03)00134-6).
- Collins, J.R., P.A. Raymond, W.F. Bohlen, and M.M. Howard-Strobel. 2013. Estimates of new and total productivity in central Long Island Sound from in situ measurements of nitrate and dissolved oxygen. *Estuaries and Coasts* 36:74–97, <https://doi.org/10.1007/s12237-012-9560-5>.
- Collos, Y., F. Mornet, A. Sciandra, N. Waser, A. Larson, and P.J. Harrison. 1999. An optical method for the rapid measurement of micromolar concentrations of nitrate in marine phytoplankton cultures. *Journal of Applied Phycology* 11:179–184, <https://doi.org/10.1023/A:1008046023487>.
- D'Ortenzio, F., H. Lavigne, F. Besson, H. Claustre, L. Coppola, N. Garcia, A. Laës-Huon, S. Le Reste, D. Malardé, C. Migon, and others. 2014. Observing mixed layer depth, nitrate and chlorophyll concentrations in the northwestern Mediterranean: A combined satellite and NO₃ profiling floats experiment. *Geophysical Research Letters* 41:6,443–6,451, <https://doi.org/10.1002/2014GL061020>.
- Dugdale, R.C., and J.J. Goering. 1967. Uptake of new and regenerated forms of nitrogen in primary productivity. *Limnology and Oceanography* 12:196–206, <https://doi.org/10.4319/lm.1967.12.2.0196>.
- Elrod, V.A., K.S. Johnson, S.E. Fitzwater, and J.N. Plant. 2008. A long-term, high-resolution record of surface water iron concentrations in the upwelling-driven central California region. *Journal of Geophysical Research* 113, C11021, <https://doi.org/10.1029/2007JC004610>.
- Eppley, R.W., and B.J. Peterson. 1979. Particulate organic matter flux and planktonic net production in the deep ocean. *Nature* 282:677–680, <https://doi.org/10.1038/282677a0>.
- Falkowski, P.G., R.T. Barber, and V. Smetacek. 1998. Biogeochemical controls and feedbacks on ocean primary production. *Science* 281:200–206, <https://doi.org/10.1126/science.281.5374.200>.
- Finch, M.S., D.J. Hydes, C.H. Claydon, B. Weigl, J. Dakin, and P. Gwilliam. 1998. A low power ultra violet spectrophotometer for measurement of nitrate in seawater: Introduction, calibration and initial sea trials. *Analytica Chimica Acta* 377:167–177, [https://doi.org/10.1016/S0003-2670\(98\)00616-3](https://doi.org/10.1016/S0003-2670(98)00616-3).
- Fischer, A.M., J.P. Ryan, and E.V. Rienecker. 2017. Fine scale mapping of the structure and composition of the Elkhorn Slough (California, USA) tidal plume. *Estuarine, Coastal and Shelf Science* 184:10–20, <https://doi.org/10.1016/j.ecss.2016.10.035>.
- Friederich, G.E., L.A. Codispoti, and C.M. Sakamoto. 1991. *An Easy-to-Construct Automated Winkler Titration System*. MBARI Technical Report No 91-6.
- Friederich, G.E., P.G. Brewer, R. Herliem, F.P. Chavez. 1995. Measurement of sea surface partial pressure of CO₂ from a moored buoy. *Deep Sea Research Part I* 42:1,175–1,186, [https://doi.org/10.1016/0967-0637\(95\)00044-7](https://doi.org/10.1016/0967-0637(95)00044-7).
- Hansen, H.P., and K. Grasshoff. 1983. *Methods of Seawater Analysis*, 2nd ed. K. Grasshoff, M. Ehrhardt, and K. Kremling, eds, Verlag Chemie, Weinheim, 347 pp.
- Harris, F.J. 1978. On the use of windows for harmonic analysis with the discrete Fourier transform. *Proceedings of the IEEE*. 66:51–83, <https://doi.org/10.1109/PROC.1978.10837>.
- Hartz, T., R. Smith, M. Cahn, T. Bottoms, S.C. Bustamante, L. Tourte, K. Johnson, and L. Coletti. 2017. Wood chip denitrification bioreactors can reduce nitrate in tile drainage. *California Agriculture* 71:41–47, <https://doi.org/10.3733/ca.2017a0007>.
- Harvey, J., Y. Zhang, and J. Ryan. 2012. AUVs for ecological studies of marine plankton communities. *Sea Technology* 53:51–54.
- Hensley, R.T., and M.J. Cohen. 2016. On the emergence of diel solute signals in flowing waters. *Water Resources Research* 52:759–772, <https://doi.org/10.1002/2015WR017895>.
- Jannasch, H.W., L.J. Coletti, K.S. Johnson, S.E. Fitzwater, J.A. Needoba, and J.N. Plant. 2008. The Land/Ocean Biogeochemical Observatory: A robust networked mooring system for continuously monitoring complex biogeochemical cycles in estuaries. *Limnology and Oceanography: Methods* 6:263–276, <https://doi.org/10.4319/lom.2008.6.263>.
- Jannasch, H.W., K.S. Johnson, and C.M. Sakamoto. 1994. Submersible, osmotically pumped analyzers for continuous determination of nitrate in situ. *Analytical Chemistry* 66:3,352–3,361, <https://doi.org/10.1021/ac00092a011>.
- Johnson, K.S. 2010. Simultaneous measurements of nitrate, oxygen, and carbon dioxide on oceanographic moorings: Observing the Redfield ratio in real time. *Limnology and Oceanography* 55:615–627, <https://doi.org/10.4319/lm.2010.55.2.0615>.
- Johnson, K.S., C.L. Beehler, and C.M. Sakamoto-Arnold. 1986a. A submersible flow analysis system. *Analytica Chimica Acta* 179:245–257, [https://doi.org/10.1016/S0003-2670\(00\)84469-4](https://doi.org/10.1016/S0003-2670(00)84469-4).

- Johnson, K.S., C.L. Beehler, C.M. Sakamoto-Arnold, and J.J. Childress. 1986b. In situ measurements of chemical distributions in a deep-sea hydrothermal vent field. *Science* 231:1139–1141, <https://doi.org/10.1126/science.231.4742.1139>.
- Johnson, K.S., J.J. Childress, R.R. Hessler, C.M. Sakamoto-Arnold, and C.L. Beehler. 1988. Chemical and biological interactions in the Rose Garden hydrothermal vent field, Galapagos spreading center. *Deep Sea Research Part A* 35:1723–1744, [https://doi.org/10.1016/0198-0149\(88\)90046-5](https://doi.org/10.1016/0198-0149(88)90046-5).
- Johnson, K.S., and H. Claustre. 2016. Bringing biogeochemistry into the Argo age. *Eos* 97, <https://doi.org/10.1029/2016EO062427>.
- Johnson, K.S., and L.J. Coletti. 2002. In situ ultraviolet spectrophotometry for high resolution and long-term monitoring of nitrate, bromide and bisulfide in the ocean. *Deep Sea Research Part I* 49:1,291–1,305, [https://doi.org/10.1016/S0967-0637\(02\)00020-1](https://doi.org/10.1016/S0967-0637(02)00020-1).
- Johnson, K.S., L.J. Coletti, and F.P. Chavez. 2006. Diel nitrate cycles observed with in situ sensors predict monthly and annual new production. *Deep Sea Research Part I* 53:561–573, <https://doi.org/10.1016/j.dsr.2005.12.004>.
- Johnson, K.S., L.J. Coletti, H.W. Jannasch, C.M. Sakamoto, D.D. Swift, and S.C. Riser. 2013. Long-term nitrate measurements in the ocean using the In Situ Ultraviolet Spectrophotometer: Sensor integration into the APEX profiling float. *Journal of Atmospheric and Oceanic Technology* 30:1,854–1,866, <https://doi.org/10.1175/JTECH-D-12-00221.1>.
- Johnson, K.S., H.W. Jannasch, L.J. Coletti, V.A. Elrod, T.R. Martz, Y. Takeshita, R.J. Carlson, and J.G. Connery. 2016. Deep-Sea DuraFET: A pressure tolerant pH sensor designed for global sensor networks. *Analytical Chemistry* 88:3,249–3,256, <https://doi.org/10.1021/acs.analchem.5b04653>.
- Johnson, K.S., and J.A. Needoba. 2008. Mapping the spatial variability of plankton metabolism using nitrate and oxygen sensors on an autonomous underwater vehicle. *Limnology and Oceanography* 53:2,237–2,250, https://doi.org/10.4319/lo.2008.53.5_part_2.2237.
- Johnson, K.S., J.N. Plant, L.J. Coletti, H.W. Jannasch, C.M. Sakamoto, S.C. Riser, D.D. Swift, N.L. Williams, E. Boss, N. Haëntjens, and others. 2017a. Biogeochemical sensor performance in the SOCCOM profiling float array. *Journal of Geophysical Research* 122:6,416–6,436, <https://doi.org/10.1002/2017JC012838>.
- Johnson, K.S., J.N. Plant, J.P. Dunne, L.D. Talley, and J.L. Sarmiento. 2017b. Annual nitrate drawdown observed by SOCCOM profiling floats and the relationship to annual net community production. *Journal of Geophysical Research* 122:6,668–6,683, <https://doi.org/10.1002/2017JC012839>.
- Johnson, K.S., S.C. Riser, and D.M. Karl. 2010. Nitrate supply from deep to near-surface waters of the North Pacific subtropical gyre. *Nature* 465:1,062–1,065, <https://doi.org/10.1038/nature09170>.
- Johnson, K.S., C.M. Sakamoto-Arnold, and C.L. Beehler. 1989. Continuous determination of nitrate concentrations in situ. *Deep Sea Research Part A* 36:1,407–1,413, [https://doi.org/10.1016/0198-0149\(89\)90091-5](https://doi.org/10.1016/0198-0149(89)90091-5).
- Karstensen, J., F. Schütte, A. Pietri, G. Krahnmann, B. Fiedler, D. Grundle, H. Hauss, A. Körtzinger, C.R. Löscher, P. Testor, and others. 2017. Upwelling and isolation in oxygen-depleted anticyclonic modewater eddies and implications for nitrate cycling. *Biogeosciences* 14:2,167–2,181, <https://doi.org/10.5194/bg-14-2167-2017>.
- Kudela, R.M., W.P. Cochlan, and R.C. Dugdale. 1997. Carbon and nitrogen uptake response to light by phytoplankton during an upwelling event. *Journal of Plankton Research* 19:609–630, <https://doi.org/10.1093/plankt/19.5.609>.
- Kudela, R.M., and R.C. Dugdale. 2000. Nutrient regulation of phytoplankton productivity in Monterey Bay, California. *Deep Sea Research Part II* 47:1,023–1,053, [https://doi.org/10.1016/S0967-0645\(99\)00135-6](https://doi.org/10.1016/S0967-0645(99)00135-6).
- Le Moigne, F.A.C., S.A. Henson, E. Cavan, C. Georges, K. Pabortsava, E.P. Achterberg, E. Ceballos-Romero, M. Zubkov, and R.J. Sanders. 2016. What causes the inverse relationship between primary production and export efficiency in the Southern Ocean. *Geophysical Research Letters* 43:4,457–4,466, <https://doi.org/10.1002/2016GL068480>.
- MacCreedy, P., and P. Quay. 2001. Biological export flux in the Southern Ocean estimated from a climatological nitrate budget. *Deep Sea Research Part II* 48:4,299–4,322, [https://doi.org/10.1016/S0967-0645\(01\)00090-X](https://doi.org/10.1016/S0967-0645(01)00090-X).
- Maiti, K., M.A. Charette, K.O. Buesseler, and M. Kahru. 2013. An inverse relationship between production and export efficiency in the Southern Ocean. *Geophysical Research Letters* 40:1,557–1,561, <https://doi.org/10.1002/grl.50219>.
- Manning, C.C., R.H.R. Stanley, D.P. Nicholson, J.M. Smith, J.T. Pennington, M.R. Fewings, M.E. Squibb, and F.P. Chavez. 2017. Impact of recently upwelled water on productivity investigated using in situ and incubation-based methods in Monterey Bay. *Journal of Geophysical Research* 122:1,901–1,926, <https://doi.org/10.1002/2016JC012306>.
- Marra, J. 2009. Net and gross productivity: Weighing in with ¹⁴C. *Aquatic Microbial Ecology* 56:123–131, <https://doi.org/10.3354/ame01306>.
- Martz, T.R., J.G. Connery, and K.S. Johnson. 2010. Testing the Honeywell Durafet for seawater pH applications. *Limnology and Oceanography: Methods* 8:172–184, <https://doi.org/10.4319/lom.2010.8.172>.
- Martz, T., U. Send, M.D. Ohman, Y. Takeshita, P. Bresnahan, H.-J. Kim, and S. Nam. 2014. Dynamic variability of biogeochemical ratios in the Southern California Current System. *Geophysical Research Letters* 41:2,496–2,501, <https://doi.org/10.1002/2014GL059332>.
- McCabe, R.M., B.M. Hickey, R.M. Kudela, K.A. Lefebvre, N.G. Adams, B.D. Bill, F.M.D. Gulland, R.E. Thomson, W.P. Cochlan, and V.L. Trainer. 2016. An unprecedented coastwide toxic algal bloom linked to anomalous ocean conditions. *Geophysical Research Letters* 43:10,366–10,376, <https://doi.org/10.1002/2016GL070023>.
- McNeil, J.D., H.W. Jannasch, T. Dickey, D. McGillicuddy, M. Brzezinski, and C.M. Sakamoto. 1999. New chemical, bio-optical and physical observations of upper ocean response to the passage of a mesoscale eddy off Bermuda. *Journal of Geophysical Research* 104:15,537–15,548, <https://doi.org/10.1029/1999JC900137>.
- Olivieri, R.A., and F.P. Chavez. 2000. A model of plankton dynamics for the coastal upwelling system of Monterey Bay, California. *Deep Sea Research Part II* 47:1,077–1,106, [https://doi.org/10.1016/S0967-0645\(99\)00137-X](https://doi.org/10.1016/S0967-0645(99)00137-X).
- Packard, D. 1989. Welcoming remarks to The Oceanography Society at its inaugural meeting. *Oceanography* 2(2):46–47, <https://doi.org/10.5670/oceanog.1989.15>.
- Pasqueron de Fommervault, O., F. D'Ortenzio, A. Mangin, R. Serra, C. Migon, H. Claustre, H. Lavigna, M. Ribera d'Alcala, L. Prieur, V. Taillandier, and others. 2015. Seasonal variability of nutrient concentrations in the Mediterranean Sea: Contribution of Bio-Argo floats. *Journal of Geophysical Research* 120:8,528–8,550, <https://doi.org/10.1002/2015JC011103>.
- Pellerin, B.A., B.D. Downing, C. Kendall, R.A. Dahlgren, T.E.C. Kraus, J. Saraceno, R.G.M. Spencer, and B.A. Bergamaschi. 2009. Assessing the sources and magnitude of diurnal nitrate variability in the San Joaquin River (California) with an in situ optical nitrate sensor and dual nitrate isotopes. *Freshwater Biology* 54:376–387, <https://doi.org/10.1111/j.1365-2427.2008.02111.x>.
- Pennington, J.T., M. Blum, and F.P. Chavez. 2016. Seawater sampling by an autonomous underwater vehicle: "Gulper" sample validation for nitrate, chlorophyll, phytoplankton, and primary production. *Limnology and Oceanography: Methods* 14:14–23, <https://doi.org/10.1002/lom3.10065>.
- Pennington, J.T., and F.P. Chavez. 2000. Seasonal fluctuations of temperature, salinity, nitrate, chlorophyll, and primary production at station H3/M1 over 1989–1996 in Monterey Bay, California. *Deep Sea Research Part II* 47:947–973, [https://doi.org/10.1016/S0967-0645\(99\)00132-0](https://doi.org/10.1016/S0967-0645(99)00132-0).
- Pennington, J.T., and F.P. Chavez. 2017. Decade-scale oceanographic fluctuation in Monterey Bay, California, 1989–2011. *Deep Sea Research Part II*, <https://doi.org/10.1016/j.dsr2.2017.07.005>.
- Pennington, J.T., G.E. Friederich, C.G. Castro, C.A. Collins, W.W. Evans, and F.P. Chavez. 2010. The northern and central California coastal upwelling system. Pp. 29–44 in *Carbon and Nutrient Fluxes in Continental Margins*. K.-K. Liu, ed., Springer-Verlag, Berlin Heidelberg.
- Pilskaln, C.H., J.B. Paduan, F.P. Chavez, R.Y. Anderson, and W.M. Berelson. 1996. Carbon export and regeneration in the coastal upwelling system of Monterey Bay, central California. *Journal of Marine Research* 54:1,149–1,178, <https://doi.org/10.1357/0022240963213772>.
- Plant, J.N., K.S. Johnson, J.A. Needoba, and L.J. Coletti. 2009. NH4-Digiscan: An in situ and laboratory ammonium analyzer for estuarine, coastal, and shelf waters. *Limnology and Oceanography: Methods* 7:144–156, <https://doi.org/10.4319/lom.2009.7.144>.
- Plant, J.N., K.S. Johnson, C.M. Sakamoto, H.W. Jannasch, L.J. Coletti, S.C. Riser, and D.D. Swift. 2016. Net community production at Ocean Station Papa observed with nitrate and oxygen sensors on profiling floats. *Global Biogeochemical Cycles* 30(6):859–879, <https://doi.org/10.1002/2015GB005349>.
- Prestigiacomo, A.R., S.W. Effler, D.A. Matthews, and L.J. Coletti. 2009. Nitrate and bisulfide: Monitoring and patterns in Onondaga Lake, New York, following implementation of nitrification treatment. *Water Environment Research* 81:466–475, <https://doi.org/10.2175/106143008X357156>.
- Ramp, S.R., J.D. Paduan, I. Shulman, J. Kindle, F.L. Bahr, and F. Chavez. 2005. Observations of upwelling and relaxation events in the northern Monterey Bay during August 2000. *Journal of Geophysical Research* 110, C07013, <https://doi.org/10.1029/2004JC002538>.
- Rode, M., S. Halbedel née Angelstein, M.R. Anis, D. Borchardt, and M. Weitere. 2016. Continuous in-stream assimilatory nitrate uptake from high-frequency sensor measurements. *Environmental Science and Technology* 50:5,685–5,694, <https://doi.org/10.1021/acs.est.6b00943>.
- Rosenfeld, L.K., F.B. Schwing, N. Garfield, and D.E. Tracy. 1994. Bifurcated flow from an upwelling center: A cold water source for Monterey Bay. *Continental Shelf Research* 14:931–964, [https://doi.org/10.1016/0278-4343\(94\)90058-2](https://doi.org/10.1016/0278-4343(94)90058-2).

- Růžička, J., and E.H. Hansen. 1975. Flow injection analyses: Part I. A new concept of fast continuous flow analysis. *Analytica Chimica Acta* 78:145–157, [https://doi.org/10.1016/S0003-2670\(01\)84761-9](https://doi.org/10.1016/S0003-2670(01)84761-9).
- Ryan, J.P., R.M. Kudela, J.M. Birch, M. Blum, H.A. Bowers, F.P. Chavez, G.J. Doucette, K. Hayashi, R. Marin III, C.M. Mikulski, and others. 2017. Causality of an extreme harmful algal bloom in Monterey Bay, California, during the 2014–2016 northeast Pacific warm anomaly. *Geophysical Research Letters* 44:5,571–5,579, <https://doi.org/10.1002/2017GL072637>.
- Ryan, J.P., M.A. McManus, and J.M. Sullivan. 2010. Interacting physical, chemical and biological forcing of phytoplankton thin-layer variability in Monterey Bay, California. *Continental Shelf Research* 30:7–16, <https://doi.org/10.1016/j.csr.2009.10.017>.
- Sakamoto, C.M., K.S. Coletti, and L.J. Coletti. 2009. Improved algorithm for the computation of nitrate concentrations in seawater using an in situ ultraviolet spectrophotometer. *Limnology and Oceanography: Methods* 7:132–143, <https://doi.org/10.4319/lom.2009.7.132>.
- Sakamoto, C.M., G.E. Friederich, S.K. Service, and F.P. Chavez. 1996. Development of automated surface seawater nitrate mapping systems for use in open ocean and coastal waters. *Deep Sea Research Part I* 43:1,763–1,775, [https://doi.org/10.1016/S0967-0637\(96\)00070-2](https://doi.org/10.1016/S0967-0637(96)00070-2).
- Sakamoto, C.M., D.M. Karl, H.W. Jannasch, R.R. Bidigare, R.M. Letelier, P.M. Walz, J.P. Ryan, P.S. Polito, and K.S. Johnson. 2004. Influence of Rossby waves on nutrient dynamics and the plankton community structure in the North Pacific subtropical gyre. *Journal of Geophysical Research* 109, C05032, <https://doi.org/10.1029/2003JC001976>.
- Santus, G., and R.W. Baker. 1995. Osmotic drug delivery: A review of the patent literature. *Journal of Controlled Release* 35:1–21, [https://doi.org/10.1016/0168-3659\(95\)00013-X](https://doi.org/10.1016/0168-3659(95)00013-X).
- Smith, J.M., K.L. Casciotti, F.P. Chavez, and C.A. Francis. 2014. Differential contributions of archaeal ammonia oxidizer ecotypes to nitrification in coastal surface waters. *The ISME Journal* 8:1,704–1,714, <https://doi.org/10.1038/ismej.2014.11>.
- Welch, P.D. 1967. The use of fast Fourier transform for the estimation of power spectra: A method based on time averaging over short, modified periodograms. *IEEE Transactions on Audio and Electroacoustics* 15:70–73, <https://doi.org/10.1109/TAU.1967.1161901>.
- Wong, C.S., N.A.D. Waser, Y. Nojiri, W.K. Johnson, F.A. Whitney, J.S.C. Page, and J. Zeng. 2002. Seasonal and interannual variability in the distribution of surface nutrients and dissolved inorganic carbon in the northern North Pacific: Influence of El Niño. *Journal of Oceanography* 58:227–243, <https://doi.org/10.1023/A:1015897323653>.
- Wong, C.S., F.A. Whitney, R.J. Matear, and K. Iseki. 1998. Enhancement of new production in the northeast subarctic Pacific Ocean during negative North Pacific index events. *Limnology and Oceanography* 43:1,418–1,426, <https://doi.org/10.4319/lo.1998.43.7.1418>.
- Wulff, T., E. Bauerfeind, and W.-J. von Appen. 2016. Physical and ecological processes at a moving ice edge in the Fram Strait as observed with an AUV. *Deep Sea Research Part I* 115:253–264, <https://doi.org/10.1016/j.dsr.2016.07.001>.
- Zhang, Y., J.G. Bellingham, J.P. Ryan, M.A. Godin. 2015. Evolution of a physical and biological front from upwelling to relaxation. *Continental Shelf Research* 108:55–64, <https://doi.org/10.1016/j.csr.2015.08.005>.

ACKNOWLEDGMENTS

We are grateful to the MBARI observatory support group for the many Monterey Bay mooring and instrument deployments; to MBARI nutrient lab personnel over the years (Gernot Friederich, Peter Walz, Marguerite Blum) for discrete nutrient analyses; to the MBARI Biological Oceanography Group (Reiko Michisaki, Tim Pennington, Marguerite Blum) for time-series sampling, analyses, and database management; to Kelly Lance for graphics support; and to the many people involved with the Marine Operations Group for shipboard and machine shop support. Funding for this project was provided by the David and Lucille Packard Foundation and the Monterey Bay Aquarium Research Institute.

AUTHORS

Carole M. Sakamoto (saca@mbari.org) is Senior Research Specialist, **Kenneth S. Johnson** is Senior Scientist, **Luke J. Coletti** is Senior Research Technician, **Tanya L. Maurer** is Research Technician, **Gene Massion** is Ocean Engineer, **J. Timothy Pennington** is Senior Research Specialist, **Joshua N. Plant** is Senior Research Technician, **Hans W. Jannasch** is Senior Research Specialist, and **Francisco P. Chavez** is Senior Scientist, all at the Monterey Bay Aquarium Research Institute, Moss Landing, CA, USA.

ARTICLE CITATION

Sakamoto, C.M., K.S. Johnson, L.J. Coletti, T.L. Maurer, G. Massion, J.T. Pennington, J.N. Plant, H.W. Jannasch, and F.P. Chavez. 2017. Hourly in situ nitrate on a coastal mooring: A 15-year record and insights into new production. *Oceanography* 30(4):114–127, <https://doi.org/10.5670/oceanog.2017.428>.